Chapter 2

Potassium Intercalated Graphite

2.1 Introduction

Graphite intercalation compounds (GICs) are a unique class of lamellar materials formed by the insertion of atomic or molecular guests between the layer planes of the host graphite. Electrical, thermal and magnetic properties can be varied by intercalation, making these materials interesting technologically. Graphite intercalation compounds exist for all alkali metals, but only the K, Rb, and Cs compounds are known to adsorb hydrogen. The maximum adsorption capacity of these materials is only around 1 wt%, but their high degree of structural ordering makes them a model system for studying hydrogen adsorption in a carbon nanostructure. They share many similarities with a chemically-modified carbon slit-pore structure, and are readily synthesized. Due to the attractiveness of potassium as a lightweight dopant for carbon adsorbents, potassium intercalated graphite is the focus of this thesis.

2.2 History

Alkali metal GICs were first prepared by Fredenhagen and co-workers in the 1920's with the compositions C_8M and $C_{16}M$ [43]. Further studies were carried out on the potassium com-

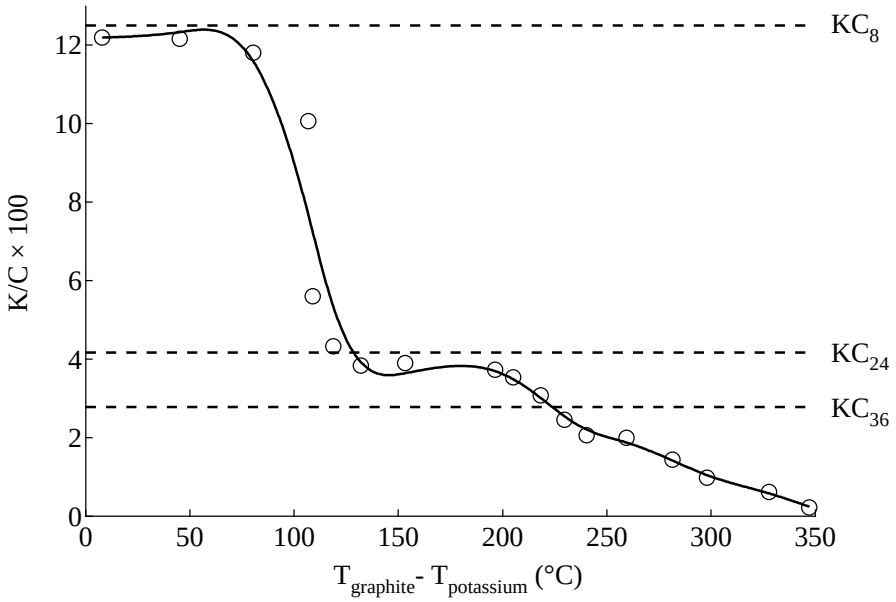

Figure 2.1: Composition of the potassium-graphite system based on the temperature difference between the graphite host and potassium vapor. Adapted from Ref. [44].

pound in the 1950's by Hérold, who developed a two-zone, vapor-phase synthesis technique where the potassium melt was kept at a constant temperature (250 ℃) while the graphite temperature was varied (250 ℃ to 600 ℃) [44]. Stoichiometric compounds of KC_8 and KC_{24} are visible as plateaus in the potassium-graphite isobar illustrated in Fig. 2.1. Structural studies of *staging* in potassium GICs were performed by Rüdorff and Schulze [45]. Discrete compositions of MC_8, MC_{24}, and MC_{36} were linked to the formation of stage 1, stage 2, and stage 3 intercalation compounds, respectively. The staging index, n, of the GIC indicates that the intercalant layer is found between every nth pair of host graphite planes. The stacking sequences in the alkali-metal GICs were further characterized by Perry and Nixon in the 1960's [46]. In the early 1960's, Saehr and Hérold discovered that KC_8 chemisorbs hydrogen at elevated temperatures up to maximum values of about $KC_8H_{0.67}$ [47]. Chemisorption was also noted for RbC_8 and KC_{24}, but not for CsC_8. Physisorption of H_2 by the stage 2 compounds of K, Rb, and Cs at low temperatures was discovered by Tamaru and co-

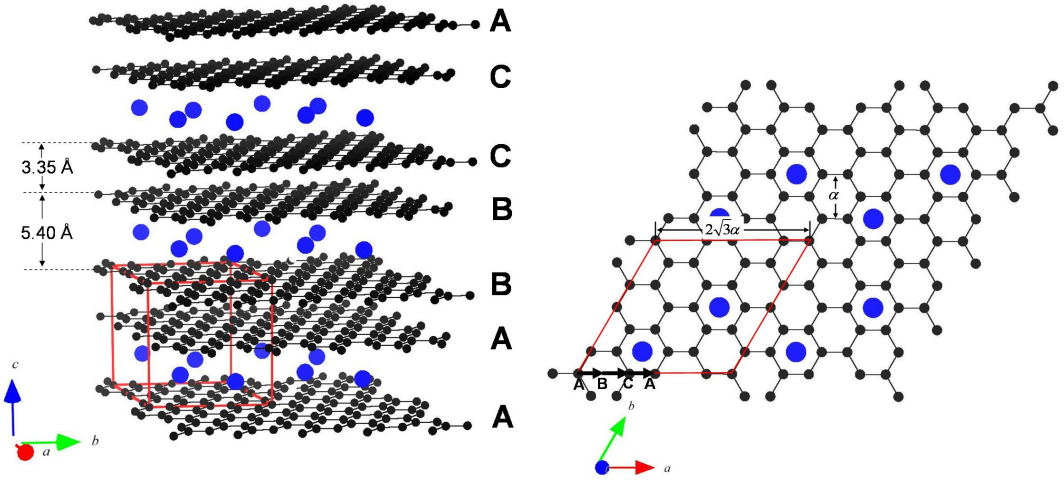

(a) Side view **(b)** Top view

Figure 2.2: Structure of KC_{24}. (a) The A|AB|BC|CA stacking sequence. (b) Possible in-plane potassium structure. Arrows from A→B→C describe the relative positions of the layer planes in the stacking sequence.

workers in the early 1970s [48]. These measurements were reproduced by a number of subsequent studies [49, 50]. The first inelastic neutron scattering studies of H_2 adsorbed in the stage-2 alkali metals compounds were performed by White and co-workers in the early 1980's [51]. Low-energy "rotational tunneling" peaks observed in the spectra indicated that the adsorbed hydrogen was in a strong anisotropic field. They were explained in terms of a one-dimensional hindered diatomic rotor model [52, 53]. By the late 1980's, a substantial body of research existed on hydrogen-alkali-metal graphite intercalation systems (see Ref. [54] and [55] for reviews on this subject). Interest in the area dwindled during the 1990's, as reflected in the small number of publications during the period. However with the emergence of hydrogen storage materials as a major topic of research, there has been a resurgence of interest in the hydrogen adsorption properties of the alkali-metal GICs.

2.3 Structure of potassium-intercalated graphite

2.3.1 Stacking sequence

Potassium GICs are formed by inserting potassium atoms into the galleries between the host graphitic layers. There are two competing forces in this system. First, the K atoms want to sit at the hexagon centers due to the strong graphite corrugation potential. This would cause the opposing basal planes to overlap exactly in an A|A sequence, where the vertical bar refers to the potassium layer. Second, the host graphite planes want to form a staggered sequence, ABAB, where half the carbon atoms in a given plane sit over the hexagon centers of the adjacent planes. It is the competition between these two driving forces that leads to the formation of discrete GIC stages. At low metal concentrations like KC_{24} and KC_{36}, it is apparently energetically favorable for metal layers to only occupy every 2^{nd} and 3^{rd} graphite gallery, respectively. For this reason, KC_{24} and KC_{36} are called the stage-2 and stage-3 compounds. The non-intercalated layers can maintain a staggered AB sequence, while the intercalated layers have an A|A sequence. If the potassium concentration is increased further, the system will eventually adopt a KC_8 stoichiometry, where the potassium atoms occupy every interlayer gallery in a close-packed 2×2 registered structure. The actual concentration of potassium within the GIC is determined by its relative chemical potential in the intercalated phase and in the vapor phase. By controlling the graphite temperature and the potassium vapor pressure (via the temperature of the melt), different potassium GIC stages can be synthesized (see Fig. 2.1).

The stage-1 compound has an orthorhombic symmetry with a known stacking sequence of AαAβAγAδA [45]. Unfortunately, the long-range stacking sequences for the stage-2 (and higher) GICs are not as well characterized. Nixon and Perry recommend the following [46]:

stage 4 ABAB|BCBC|CACA|

stage 3 ABA|ACA|A

stage 2 AB|BC|CA|A

An *in situ* X-ray diffraction study of the potassium GIC was actually able to identify stages 1 to 7, observing no evidence of microscopic mixing of the different stages [56]. The nominal stacking sequence of KC_{24} is illustrated in Fig. 2.2b, where the arrow from A to B indicates how the plane "A" is shifted with respect to the plane "B." When potassium is inserted into the host graphite, the interlayer spacing expands from 3.35 Å to 5.40 Å in the potassium-containing galleries, as indicated in Fig. 2.2a. The unintercalated galleries remain at 3.35 Å.

2.3.2 In-plane potassium structure

At room temperature, the potassium atoms are disordered within the graphite galleries and are often described in terms of a two-dimensional liquid [58]. A series of low-temperature phase transformations are known to occur in KC_{24} in which both the in-plane structure and stacking sequence assume long-range order [59, 60]. Unfortunately, the in-plane potassium structure has not been conclusively determined. While the stage-1 compound KC_8 has a commensurate (2×2) $R\,0°$ in-plane structure, stage-n compounds (KC_{12n} for $n > 1$) have a lower potassium density in each layer. The potassium atoms are likely to be commensurate with the host graphite at low temperatures, but simple periodic registered structures are not consistent with X-ray data [57, 61]. Graphite has a honeycomb lattice structure, so the minimum-energy sites at the hexagon centers form a triangular lattice. It would make sense to populate this triangular lattice in a periodic fashion to give the correct KC_{24} stoichiometry. The $\left(\sqrt{12} \times \sqrt{12}\right)$ $R\,30°$ structure depicted in Fig. 2.3a gives the correct

24:1 stoichiometry, but it is not consistent with X-ray diffraction patterns [61]. Another idea is to take an incommensurate close-packed potassium monolayer with a liquid-like separation of roughly 6 Å, rotate the layer around the c-axis by an arbitrary angle, and then relax the potassium atoms into the nearest hexagon centers [57]. This relaxed close-packed structure contains nearest-neighbor distances of $2a$, $\sqrt{7}a$, and $3a$ and has reasonable agreement with single-crystal X-ray data [61]. An example is illustrated in Fig. 2.3c.

Unlike KC_{24}, the low-temperature in-planes structures of RbC_{24} and CsC_{24} are well

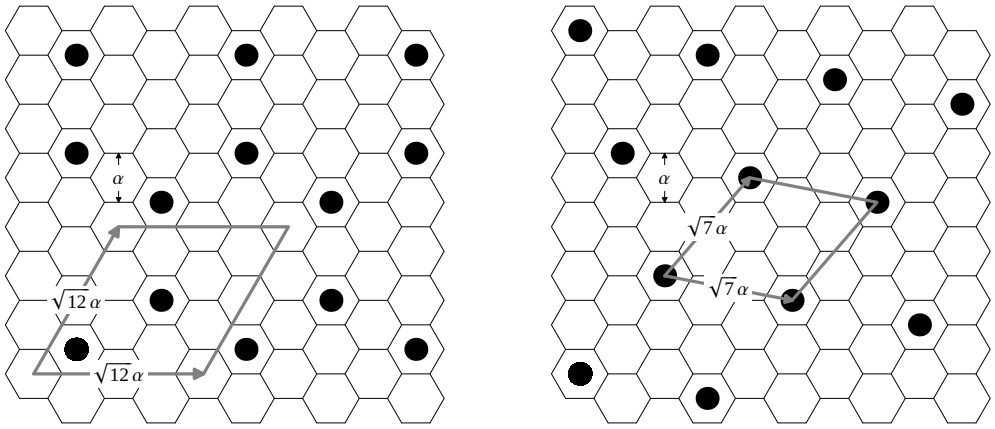

(a) $\left(\sqrt{12} \times \sqrt{12}\right) R\,30°$ structure

(b) $\left(\sqrt{7} \times \sqrt{7}\right) R\,19.11°$ structure

(c) Relaxed Close-Packed

Figure 2.3: In-plane potassium structures in registry with the graphite host. The $\left(\sqrt{12} \times \sqrt{12}\right)$ structure corresponds to a KC_{24} stoichiometry. The $\left(\sqrt{7} \times \sqrt{7}\right)$ structure has a KC_{28} stoichiometry. The relaxed close-packed structure (adapted from Ref. [57]) consists of a close-packed potassium layer which has been rotated in-plane and relaxed into the nearest hexagon centers.

described by a domain model [62, 63]. As illustrated in Fig. 2.4, they contain locally commensurate $\left(\sqrt{7} \times \sqrt{7}\right) R\,19.11°$ patches surrounded by domain walls. The idealized $\sqrt{7} \times \sqrt{7}$ structure (see Fig. 2.3b) has been the basis of most *ab initio* studies of the H_2/KC_{24} system [64,65]. Unfortunately the $\sqrt{7} \times \sqrt{7}$ structure has a KC_{28} stoichiometry. In the domain model the boundary regions have a greater alkali metal density, causing the total stoichiometry to even out at about 24 to 1. However, the domain model with discommensurations has not been consistent with single-crystal diffraction data measured on KC_{24} [61]. It seems that the relaxed close-packed structure, an analogue of the random lattice-gas model, is the most compelling structural model for the in-plane potassium arrangement.

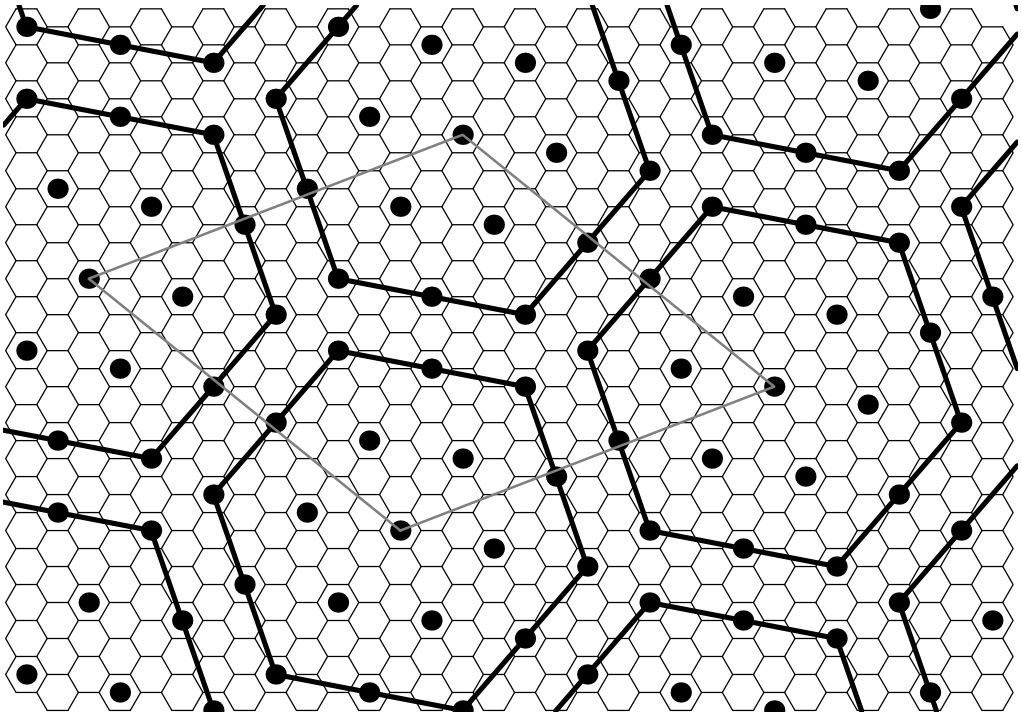

Figure 2.4: Domain model for CsC_{24} in which $\sqrt{7} \times \sqrt{7}$ islands are separated by domain walls, or discommensurations. Adapted from Ref. [62].

2.4 Properties of potassium-intercalated graphite

Graphite is a semi-metal with a complex band structure. It has only about 10^{-4} charge carriers per carbon atom. Alkali metal GICs, like KC_{24}, are classified as *donor* compounds because the metal atoms donate charge to the graphite conduction band. This results in a large increase in both the in-plane conductivity (σ_a) and c-axis conductivity (σ_c). Due to the layered structure of GICs, there is also considerable anisotropy in the charge transport properties. For KC_{24}, the c-axis conductivity is about 24 times larger than for pristine graphite, and the anisotropy factor σ_a/σ_c is about 860 [66]. Partial charge transfer from potassium to the empty graphite bands appears to be experimentally established [67].

Hydrogen physisorption in KC_{24}, RbC_{24}, and CsC_{24} has been previously investigated [48]. The Li and Na compounds do not physisorb hydrogen because the widths of the metal-containing galleries are too small. Notably, KC_{24} has molecular sieving properties in which it adsorbs smaller molecules (e.g., hydrogen), but does not adsorb larger molecules (e.g. methane). Quantum sieving effects are also present in KC_{24}, in which D_2 is adsorbed preferentially over H_2 [50]. The hydrogen adsorption characteristics depend on the quality of the starting graphite. The best adsorption is obtained for high purity, natural flake crystalline graphite. As the amount of amorphous impurities in the starting graphite increases, the H_2 adsorption amount decreases [68].

Hydrogen is adsorbed into the metal-containing layers of KC_{24}, forming a quasi-two-dimensional binary solution with potassium. There is no evidence for anything other than a monolayer structure in which the potassium and H_2 are mixed. The potassium-containing layer expands from 5.4 Å to 5.6 Å following hydrogen adsorption. This is an interlayer expansion of almost 5 %, which is surprisingly large, but is still too small to support a bilayer or

trilayer H_2-K-H_2 structure. There is also no evidence for H_2 dissociation during physisorption, as verified by a chromatographic analysis of an H_2/D_2 mixture [48]. It is unclear whether the potassium superstructure is rigid, or whether it undergoes rearrangement after the introduction of hydrogen.

Interactions between hydrogen and KC_{24} are likely to have both dispersion and electrostatic components. Charge transfer from potassium to graphite results in a strongly polarized potential field which can have significant charge-quadrupole and charge-induced-dipole interactions with the adsorbed H_2 molecules. However, charge density surrounding the potassium atoms, and present in the bounding graphite layers, can also lead to an enhanced dispersion interaction with the H_2 molecule. Computational studies report an enhancement of the energy for the H_2 interaction with an alkali-doped graphene surface, due largely to the increased electron density on the surface surrounding the alkali impurity [39, 69]. The reported H_2 isosteric heat on KC_{24} is $8.4\,\mathrm{kJ\,mol^{-1}}$, about twice as large as for adsorption on bare graphite [48]. It is also known that the in-plane resistivity in $KC_{24}(H_2)_x$ is larger than in KC_{24} [55]. This is explained by the observed c-axis expansion, which effectively reduces the in-plane carrier density. Charge back-donation from the conducting π bands to the hydrogen σ^* anti-bonding orbital seems unlikely and has not been conclusively demonstrated [54, 55].

2.5 Synthesis of KC_{24} samples

Samples of KC_{24} used in this work were synthesized using a modified single-temperature-zone technique. The starting materials were thermally purified natural flake graphite (Superior Graphite Co., 99.95–99.99% purity, 50 mesh) and potassium metal (Alfa Aesar, 99.9%). Since the starting graphite had already been subject to a high-temperature purifi-

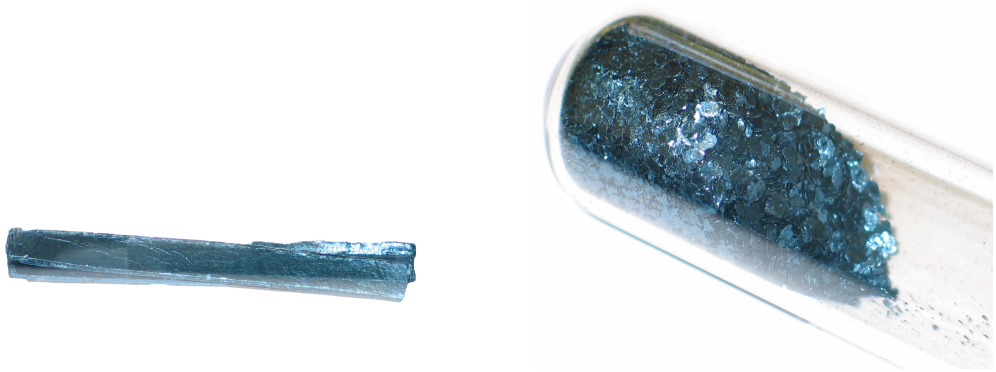

(a) Grafoil **(b)** Flake graphite

Figure 2.5: Samples of KC_{24} synthesized from Grafoil and natural flake graphite.

cation process, it was not necessary to puruse further purification.[1] Stoichiometric amounts of graphite and potassium were weighed out inside an argon glovebox, transferred to a glass ampoule, and connected to a threaded glass vacuum valve with an O-ring sealed Teflon plug. The ampoule was then evacuated to 60 Torr and sealed with an oxygen torch. Samples were heated at 300 °C for 24 h to 48 h and shaken occasionally to ensure homogeneity. This last step was required to make sure that a homogenous stage-2 compound was produced instead of a mixture of stage-1 and higher-stage compounds. Samples produced with this method are pictured in Fig. 2.5.

Measuring out exact amounts of potassium was probably the trickiest part of the synthesis and required a certain amount of trial by error. Coating the surface of individual potassium pieces with a layer of flaked graphite prevented them from sticking to the ampoule walls during loading. By measuring the initial and final masses of both the ampoule and the source graphite, it was possible to determine the exact amounts of both the potassium and the graphite. Further, I found that using a 22:1 molar ratio of graphite to potassium produced the best samples. A thin film of potassium was typically plated onto the glass which meant that not all of the loaded potassium was necessarily intercalated into the sam-

[1] As a precaution, the graphite was outgassed under dynamic vacuum at 200 °C to remove any residual water that may have been adsorbed on the surface.

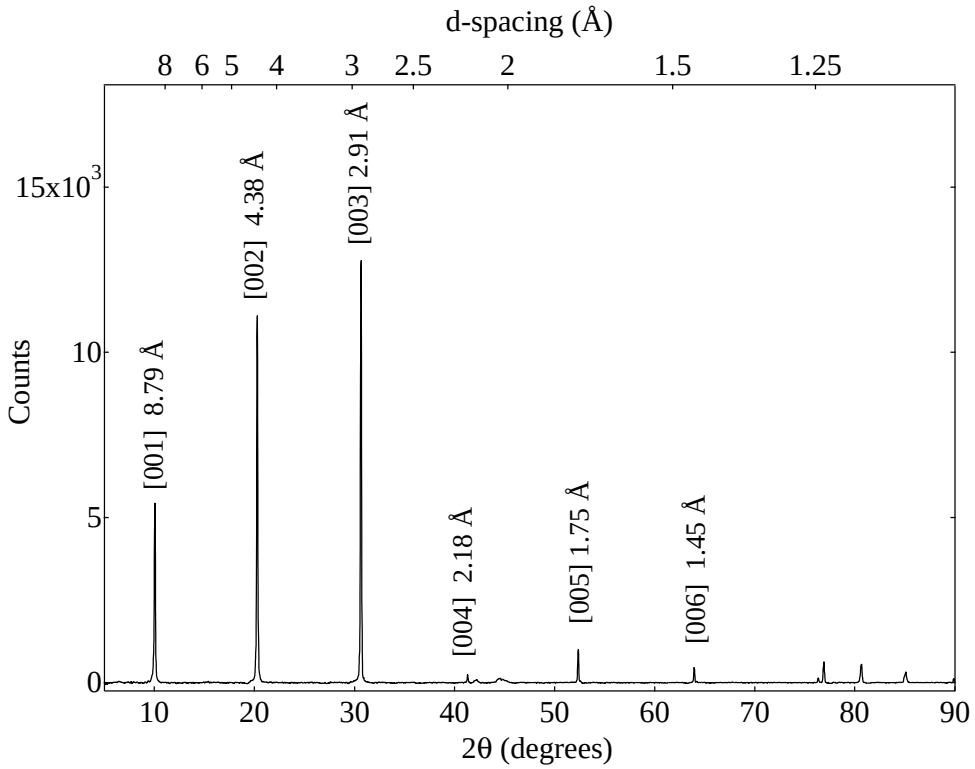

Figure 2.6: Powder XRD pattern of KC_{24} at room temperature.

ple. Samples of RbC_{24} and CsC_{24} were synthesized using the same method, substituting for different alkali metals. An additional KC_{24} sample was synthesized from a nuclear grade Grafoil® (99.5% graphite, 0.152 cm thickness) starting material used without further purification. The Grafoil-based sample had a stoichiometry of $KC_{21.7}$ and a helium density of $2.03(6)\,\mathrm{g\,ml^{-1}}$.

2.6 Characterization of KC_{24} samples

2.6.1 Powder X-ray diffraction

Powder X-ray diffraction (XRD) measurements verified the phase purity of KC_{24} samples synthesized from natural flake graphite. Rubidium and cesium GIC samples were also characterized. The XRD patterns were collected on a PANalytical X'pert PRO X'celerator

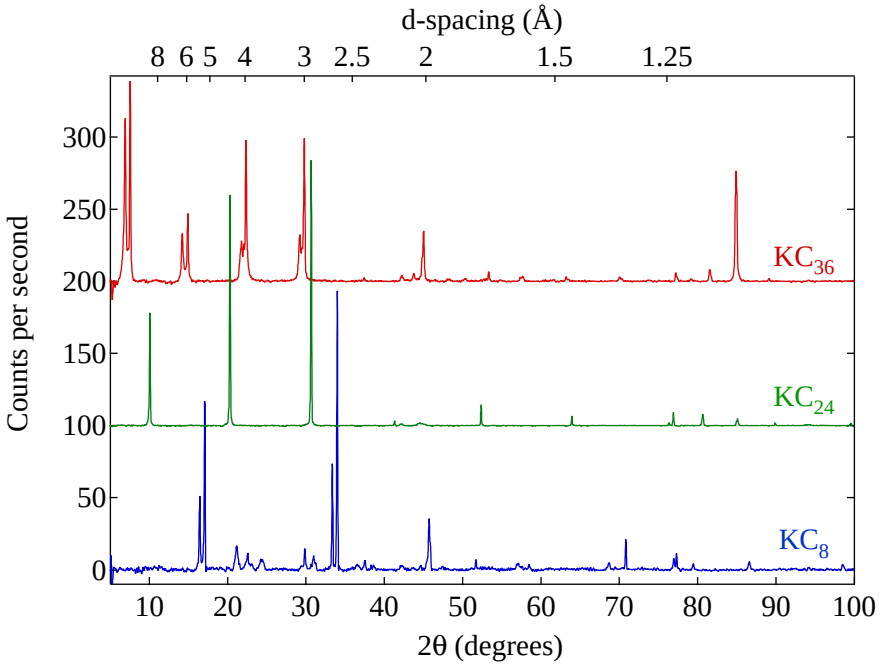

Figure 2.7: Comparison of the powder XRD patterns of stage-1, stage-2, and stage-3 potassium graphite intercalation compounds.

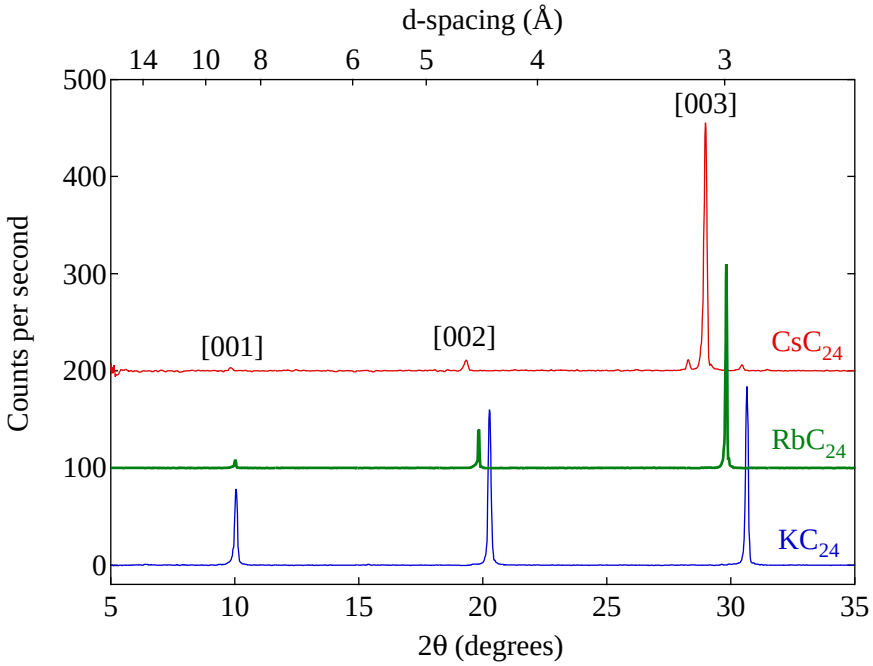

Figure 2.8: Comparison of the powder XRD patterns of KC_{24}, RbC_{24}, and CsC_{24} graphite intercalation compounds.

Table 2.1: Lattice parameters of synthesized graphite intercalation compounds

Sample	Lattice parameter(Å)[a]	Interlayer spacing (Å)[b]
KC_{24}	8.76 ± 0.02	5.41 ± 0.02
KC_{36}	12.1 ± 0.30	5.40 ± 0.30
RbC_{24}	8.95 ± 0.08	5.60 ± 0.08
CsC_{24}	9.25 ± 0.05	5.90 ± 0.05

[a] This c-axis lattice parameter gives the combined interlayer width of an AB|B sequence for a stage-2 compound (or an ABA|A sequence for a stage-3 compound). Values were averaged from the 001, 002, and 003 reflections.

[b] The interlayer spacing refers to the width of a metal-containing layer. It is equal to the c-axis lattice parameter minus the widths of the non-intercalated layers (e.g., 3.35 Å for a single non-intercalated layer.)

diffractometer using Cu Kα radiation ($\lambda = 1.5418$ Å). Samples were sealed within an argon atmosphere inside 1.5 mm ID glass capillary tubes using a low vapor pressure vacuum epoxy (TorrSeal™, Varian Inc.), and mounted onto a specialized capillary goniometer. I chose not to spin the capillary holder during data collection in order to not disturb the alignment. All measurements were collected at room temperature. An XRD pattern for KC_{24} is shown in Fig. 2.6. The dominant features in the KC_{24} diffraction pattern are the [00l] basal-plane reflections, which indicate a repeat distance of 8.76 ± 0.02 Å. This gives an interlayer spacing of $d = 8.76 - 3.35 = 5.41$ Å, compared to the literature value of 5.40 Å [45]. The higher order reflections follow the expected d_{001}/l spacing. Reflections with non-zero h and k are not visible in the powder diffraction pattern.

For comparison, additional powder XRD patterns were collected for the stage-1 and stage-3 potassium GICs. This data is pictured in Fig. 2.7. As desired, there are no Bragg peaks from either the stage-1 or stage-3 impurities in the prepared KC_{24} sample. The presence of a fine structure in the diffraction peaks of KC_8 and KC_{36} is very likely to be an artifact from the large diameter of the XRD capillary tubes. If two graphite flakes meet the same diffraction condition but are separated by a distance of 1.5 mm, the resulting diffraction peaks could easily be shifted by about 1°, producing the observed fine structure. Further,

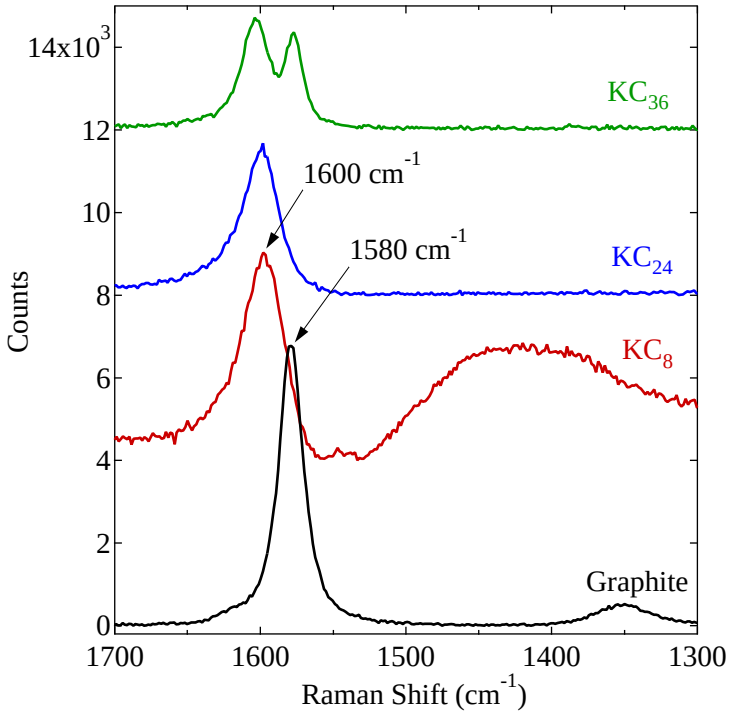

Figure 2.9: Raman scattering spectra of the potassium graphite intercalation compounds at room temperature. Measured scattering was from individual flakes.

the capillary tubes were usually not aligned perfectly on the goniometer head (alignment was done "by eye"), creating a second, perhaps larger, source of error. Admittedly, using wide-diameter capillary tubes was not the most accurate way to determine lattice parameters. Graphite flakes do not fit into smaller diameter capillary tubes without first being ground up (which I wanted to avoid for these materials). Nevertheless, powder XRD provided us the qualitative information we needed: KC_{24} samples were synthesized correctly and were not contaminated by impurities from stage-1 or stage-3. Additional powder XRD patterns were collected for RbC_{24} and CsC_{24} samples, as illustrated in Fig. 2.8. A summary of lattice parameter data for all of the synthesized alkali metal GICs is provided in Table 2.1.

2.6.2 Raman spectroscopy

Raman spectroscopy was used as an alternative method of verifying the phase purity of prepared KC_{24} samples. Measurements were collected on Renishaw M1000 Micro-Raman spectrometer, operating at $1\,cm^{-1}$ spectral resolution with a 514.5 nm argon laser. Samples were sealed in 1.5 mm glass capillary tubes and data was collected at room temperature. Data for KC_8, KC_{24}, and KC_{36} are displayed in Fig. 2.9. The peak at around $1600\,cm^{-1}$ is typically assigned to the E_{2g2} mode of graphite where the graphite layer is bounded by an intercalant layer on one side and a graphite layer on the other side [70]. The peak near $1580\,cm^{-1}$ is typically assigned to an E_{2g2} mode where the layer is bounded on both sides by a graphite plane. As expected, the $1580\,cm^{-1}$ mode is present for pristine graphite and for KC_{36} (which contains an intercalant layer in every third gallery). The $1600\,cm^{-1}$ mode is present as expected in both the KC_{24} and KC_{36} spectra, though it is unclear why it is also present in KC_8 (which contains an intercalant in every layer).

2.6.3 Neutron diffraction

Neutron diffraction work on a D_2/KC_{24} system was performed at the NPDF beamline at the Lujan Center, located at the Los Alamos National Laboratory.[2] Approximately 1 g of powder was loaded into a leak-tight vanadium sample can with an attached capillary line for dosing with D_2 gas. The diffraction pattern of KC_{24} without D_2 was measured at both 298 K and 35 K. Interestingly, there is no notable difference in these two diffraction patterns except for small shifts due to thermal expansion.[3] Deuterium gas was introduced to the sample at 300 K, and the temperature was lowered at intervals down to a base temperature

[2] Measurements performed by C. C. Ahn, B. Fultz, and R. Yazami in 2001 [71].

[3] The observable powder diffraction peaks are apparently not sensitive to the order-disorder transformation that occurs in the potassium intercalate layers at low temperatures.

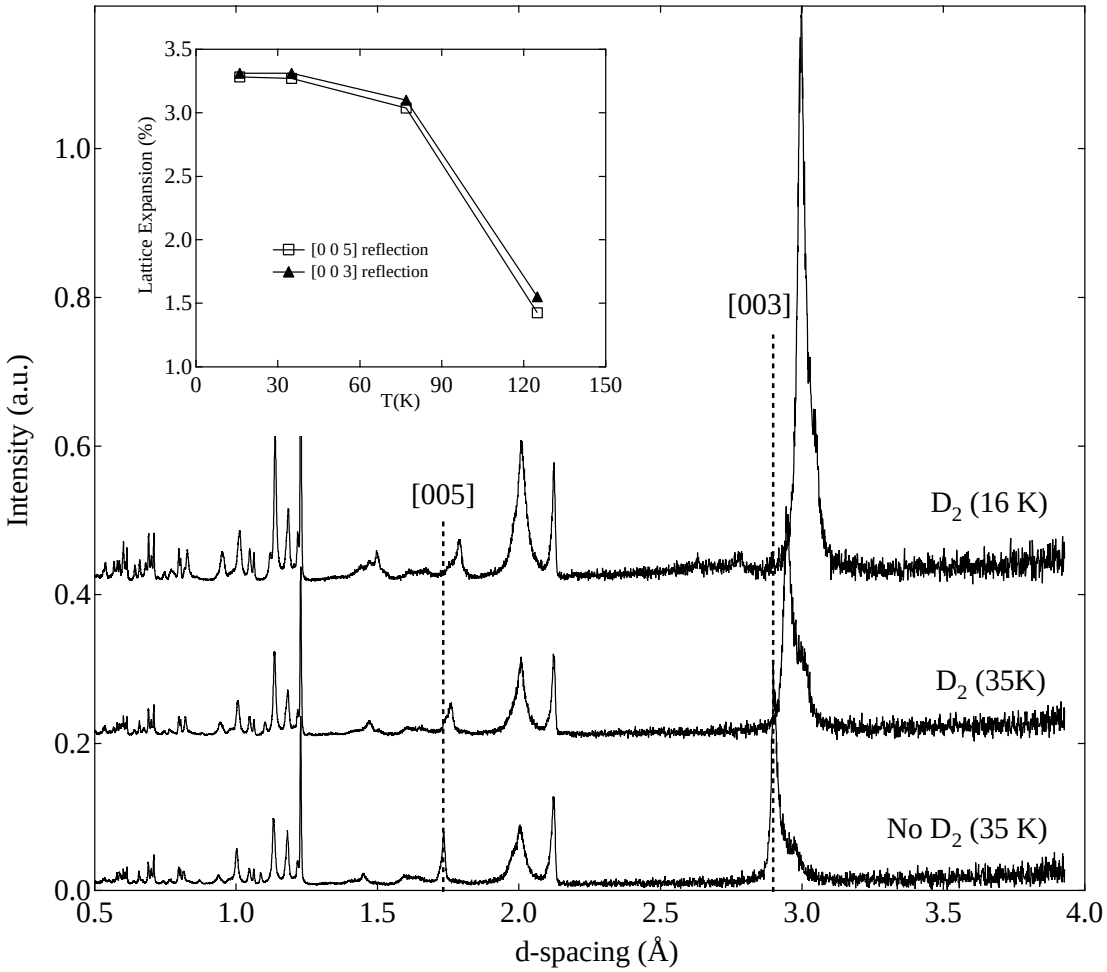

Figure 2.10: Neutron diffraction pattern for KC_{24} powder. Displayed data is for a KC_{24} sample at 35 K, and a $KC_{24} + D_2$ sample at 35 K and 16 K. Inset shows the percent increase of the *c*-axis lattice parameter from the [003] and [005] peak-shifts of the deuterated sample as a function of temperature. Diffraction patterns from 77 K and 120 K are not pictured.

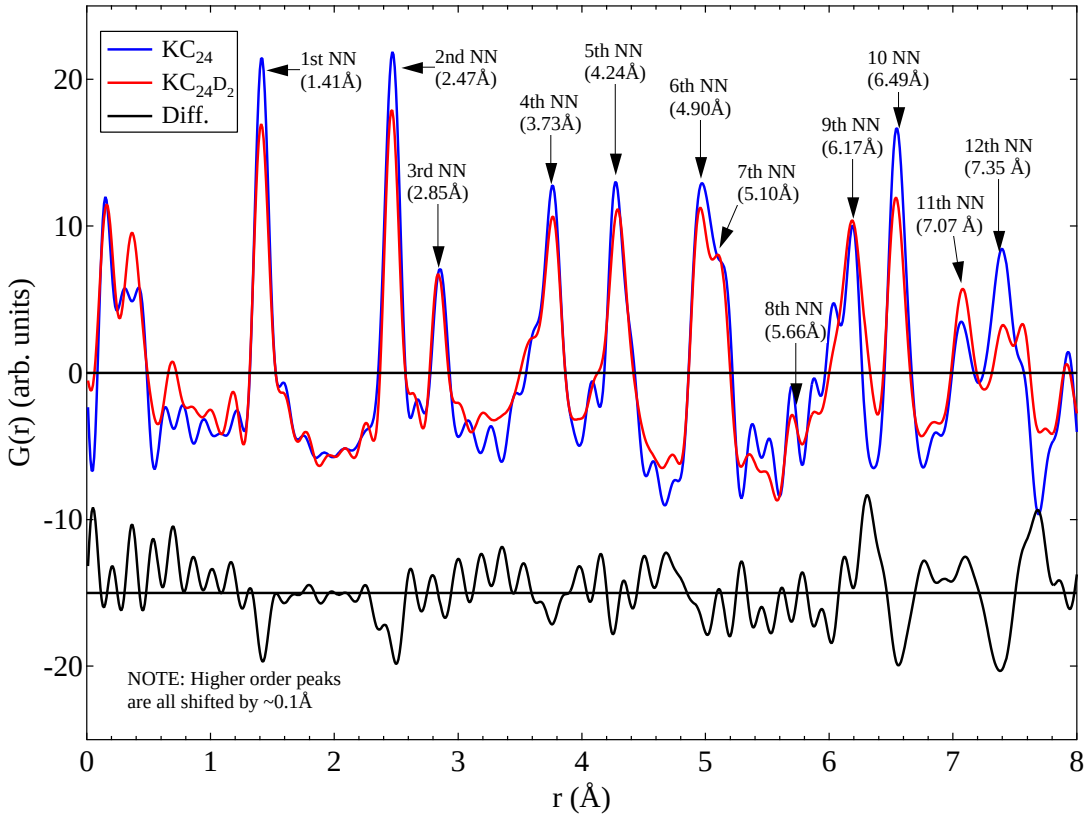

Figure 2.11: Pair distribution function calculated from the KC_{24} and $KC_{24} + D_2$ powder neutron diffraction patterns at 35 K. The difference spectrum is also displayed at a negative offset along the y-axis. All major peaks are assigned to carbon nearest-neighbor distances within a graphite plane.

of 16 K. The c-axis repeat distance, as determined from the [003] and [005] peaks, increases from 8.69 Å for the un-deuterated sample to 8.97 Å for the deuterated sample at 16 K (Fig. 2.10). This corresponds to a 5 % expansion in the interlayer spacing from 5.34 Å to 5.62 Å, roughly consistent with previous results [48].

Pair distribution functions (PDF) for both KC_{24} and KC_{24}+D_2 were back-transformed from the diffraction profiles of each sample collected at 35 K. The results are displayed in Fig. 2.11. Peaks in the PDF can almost entirely be assigned to nearest-neighbor distances of carbons in a graphite layer. Referring to Fig. 2.3c, the expected K−K distances are roughly 4.9 Å, 6.47 Å, and 7.34 Å. Deuterium might be expected to have similar nearest-neighbor distances at low loadings. Interestingly, there are some areas of intensity in the difference plot around 6.3 Å and 7.8 Å which may correspond to the latter two of the expected distances. Unfortunately, it is difficult to draw any information about either the potassium or deuterium structures from the PDF plot.